

Research Article www.acsami.org

Tunable Surfaces and Films from Thioester Containing **Microparticles**

Alina M. Martinez, Lewis M. Cox, Amir Darabi, Nicholas J. Bongiardina, and Christopher N. Bowman*



Cite This: ACS Appl. Mater. Interfaces 2022, 14, 27177-27186



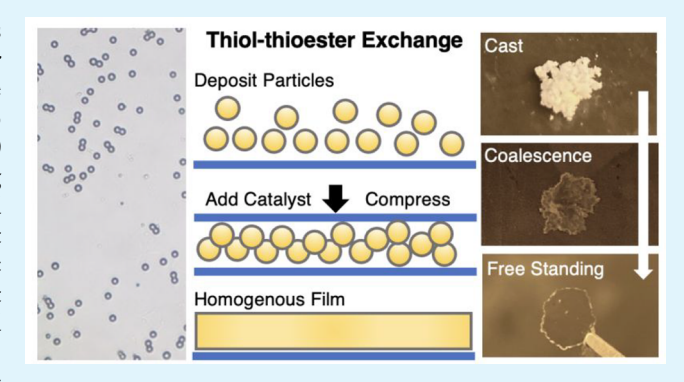
ACCESS I

Metrics & More



Supporting Information

ABSTRACT: Reported here, thioester containing microparticles were designed with 40% excess thiol to enable thiol-thioester exchange to facilitate the formation of cohesive films from the particles. A thiol-Michael dispersion polymerization was used to generate thioester containing microparticles with a diameter of 4.0 \pm 0.4 μ m. The particles were then swollen with a base at varying concentrations to activate the thiol-thioester exchange and subsequently compressed between two glass slides. Resultant films were characterized over time with profilometry and atomic force microscopy (AFM) to infer particle coalescence at different catalyst loadings and times. Tensile tests were performed confirming the structural integrity of the particle-based films. Furthermore, microparticles were welded to a nondynamic



network demonstrating feasibility in potential applications to generate materials containing differing mechanical properties. Being able to control the functionality of particles, and thus mechanical properties of the resultant films, is also important for applications in coatings, adhesives, and 3D printing where spatial patterning or selective material property control is needed.

KEYWORDS: particle coalescence, covalent adaptable network, thiol-thioester exchange, spatial patterning, spatial deposition, interfacial welding

INTRODUCTION

Selective control over material composition is important in a multitude of applications including 3D printing, biological applications,² and composites.³ The precision and selectivity with which materials can be deposited is a significant challenge in controlling compositional properties. An example of selective deposition is direct-write 3D printing, which is capable of depositing materials with micron-scale resolution.⁴ Investigating chemistries for the writing ink in these processes is important to understanding and controlling resultant network hetero- or homogeneity. Often, interfaces between materials of same or varying composition result in failure. 5-7 Polymeric interfacial welding is a physical or chemical process, achieved between two polymers of the same or differing chemistries. Physical interfacial welding is a result of polymer chain entanglements,8 while chemical welding includes surface reactions or covalent bond rearrangements. Self-healing at these interfaces often restores the integrity or capability of the chemistry(ies) chosen. Distinctly, the latex coalescence process can be thought about as a physical interfacial welding process, with increased polymer chain entanglements resulting in linear polymeric films. 10 Particle coalescence of linear polymers has been studied with the resulting materials demonstrating homogeneous properties. 11-13 Although, the noncross-linked characteristics of these materials make them degradable.

Instances of coalesced cross-linked particles have been demonstrated but have difficulty reaching a homogeneous network structure. One processing method includes the vulcanization of rubber particles. 14,15

Covalent adaptable networks (CANs) have been at the forefront of chemistries used to address issues of homogeneity, intermolecular network exchange, self-healing, and reprocessability. As typically demonstrated in bulk films, interfacial welding is widely used as a demonstration for CAN capabilities. 16,17 A variety of dynamic covalent chemistries (DCCs) have been demonstrated to promote self-healing or be capable of interfacial welding including Diels-Alder, ^{18,19} addition-fragmentation chain-transfer, ^{20,21} transesterification, 22,23 and the thiol-thioester exchange. 24 With this understanding, CANs have also become an attractive means to control resultant material properties to address interfacial complexities in addition to polymer welding, for the applications listed in the first paragraph. Some of these

Received: March 23, 2022 Accepted: May 23, 2022 Published: June 6, 2022





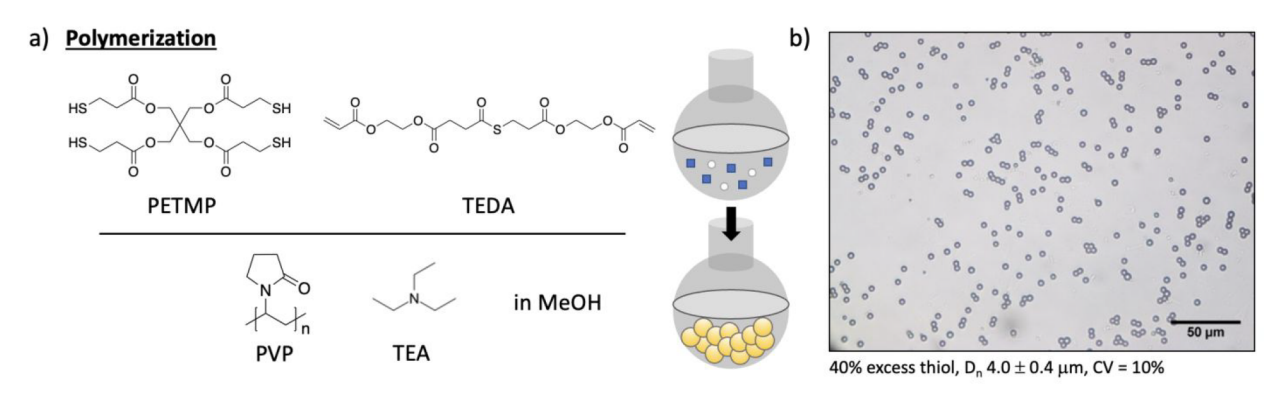


Figure 1. (a) Monomers and reaction constituents for the thiol-Michael dispersion polymerization. (b) Optical microscopy of thioester containing microparticles.

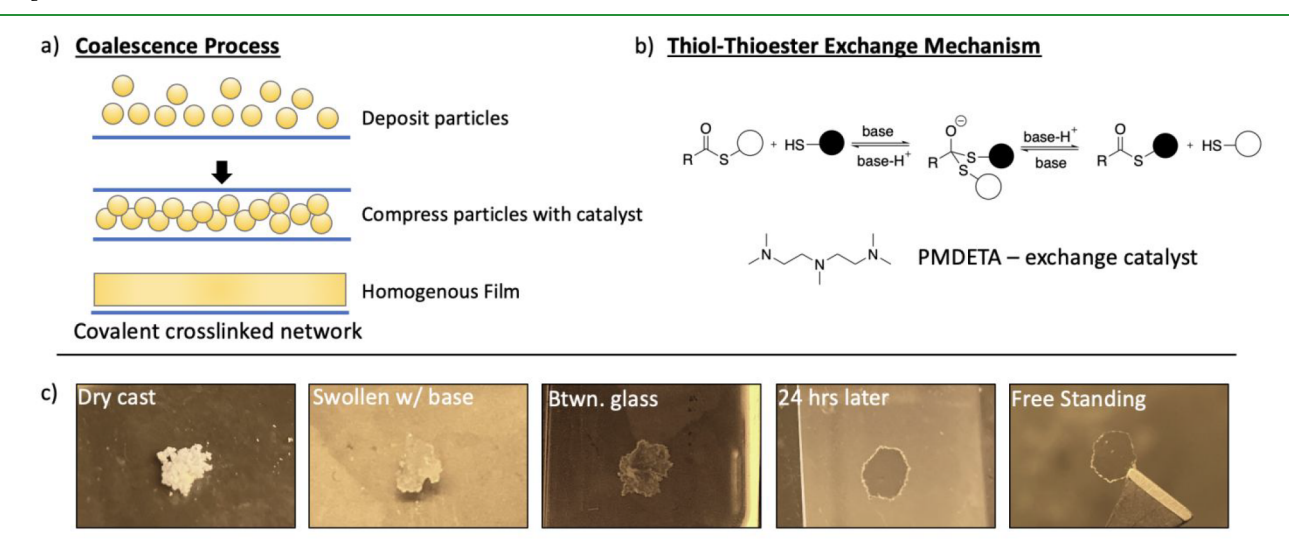


Figure 2. (a) Schematic of the particle deposition and coalescence process. (b) Mechanism for the thiol-thioester exchange. (c) Images from the actual particle casting and coalescence process over time.

DCCs include dynamic disulfide and transesterification-based epoxies for 3D printing, ^{25,26} thiol—thioester exchange for hydrogels, ²⁷ and addition—fragmentation chain-transfer functionalized nanoparticles. ²⁸ Some reports have demonstrated successful annealing of CAN-particles into a coalesced film. Huang et al. utilized boronic ester exchange as a DCC in polymer microparticles coated with carbon nanotubes to create a cohesive network structure with embedded functionality.²⁹ Another report by Lu and co-workers utilized the transesterification reaction to study the coalescence of vitrimer particles of different sizes, concluding particles of smaller dimension result in materials with higher mechanical properties.30

By incorporating CANs, networks are able to realize homogeneous properties. CANs also enable reprocessability or recyclability depending on the chemistry and conditions. Integrating CANs into particles to induce coalescence provides a novel avenue to achieve homogeneity in resulting crosslinked structures. Utilizing CAN-particles as writing inks would offer advantages such as selective deposition, which results in better structural integrity during deposition compared to liquid resins. Here, interfacial coalescence of CAN-microparticles containing a thioester network capable of thiol-thioester exchange is demonstrated. The network contains free thiols, which exchange with the thioester backbone via a basedcatalyzed mechanism. By activating the DCC within the CAN,

particles are transformed into robust polymer films with comparable mechanical integrity to polymer films made directly from monomers. The mechanism for coalescence is driven by interparticle bond exchange. By selectively varying the catalyst loading and processing time, control over the particle coalescence to a film is achieved and evaluated with UV-visible spectroscopy (UV-vis), optical microscopy, profilometry, atomic force microscopy (AFM), and tensile testing. Furthermore, we demonstrate the ability to create a cohesive polymer film with selectively deposited particles resulting in spatially controlled mechanical properties.

RESULTS AND DISCUSSION

Here, amorphous cross-linked CAN-microparticles are designed and synthesized, achieving selectively controllable bond exchange to activate particle coalescence resulting in crosslinked film formation. The particles include catalyst activated thiol-thioester exchange, with excess thiols designed into the network. To generate cross-linked particles capable of thiolthioester exchange, a thiol-Michael dispersion polymerization was performed in MeOH utilizing a tetrafunctional thiol (PETMP) and a thioester diacrylate monomer (TEDA) at a 1.4 to 2 monomer molar ratio, leaving a 40% excess of thiol (Figure 1a). Polyvinylpyrrolidone (PVP) was added at 50 wt % with respect to monomers to stabilize microparticle formation. A base, triethylamine (TEA) was used to catalyze the

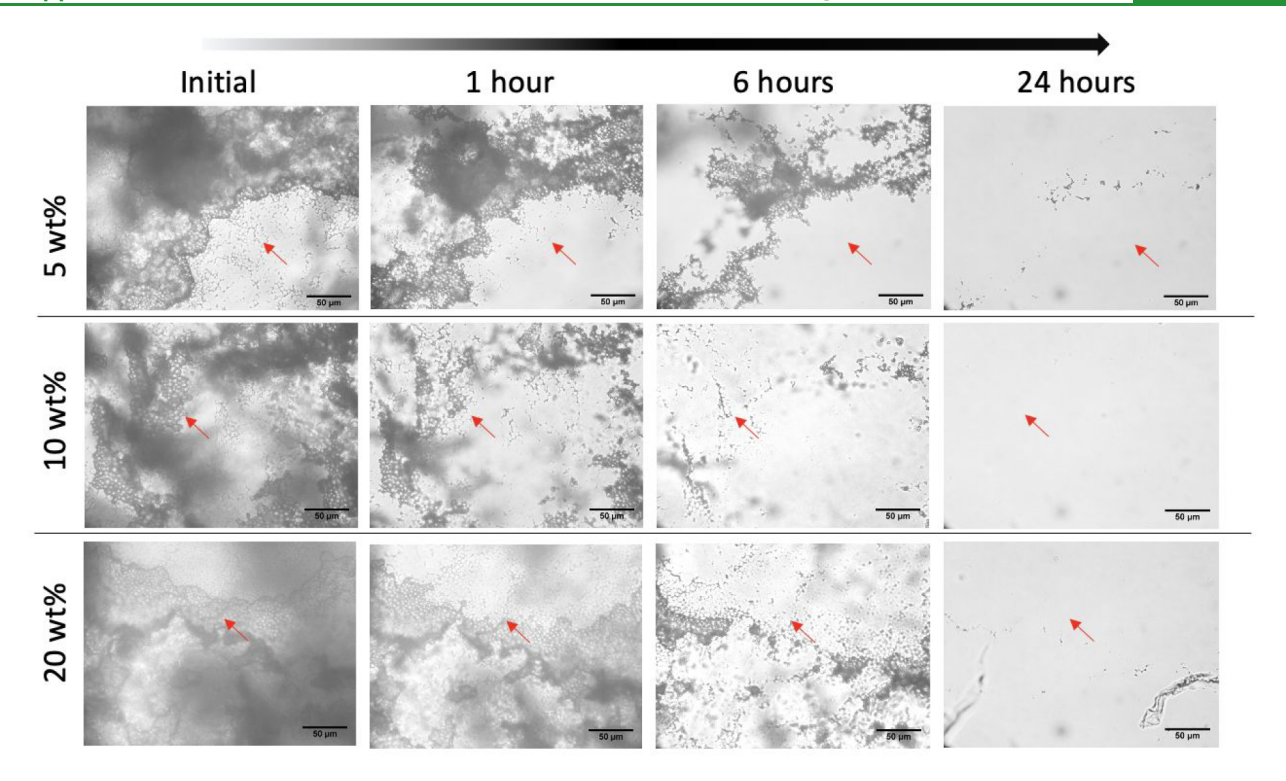


Figure 3. Optical microscopy of the particle coalescence process over time at varying concentrations of PMDETA: 5, 10, and 20 wt % loading. Imaged immediately after swelling, 1, 6, and 24 h after swelling displaying particle coalescence through the bulk of the film over time. A red arrow has been placed in the same position for each catalyst loading as a reference to monitor particle coalescence.

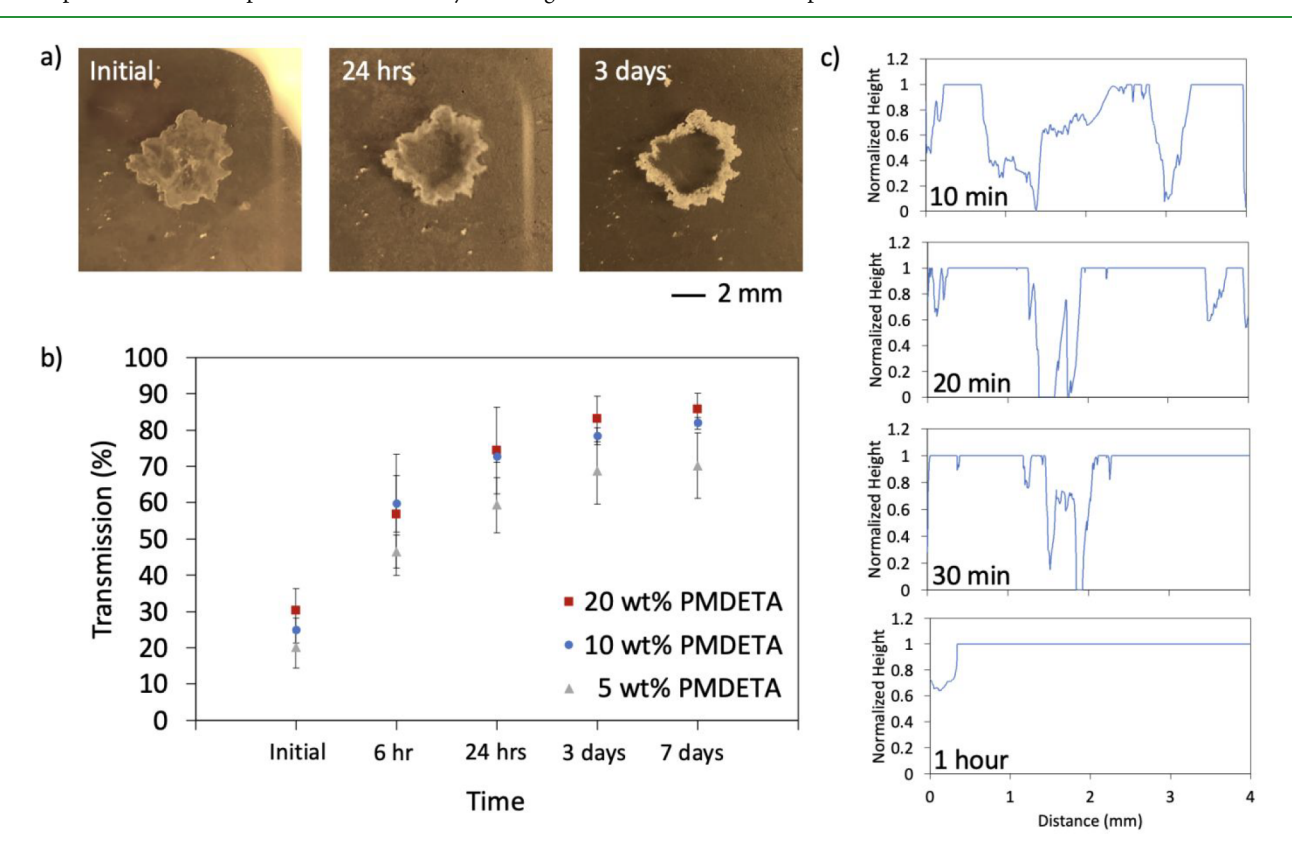


Figure 4. (a) Images of film undergoing particle coalescence over time at 20 wt % PMDETA loading. (b) UV—vis for particle coalescence over time at 5, 10, and 20 wt % PMDETA loadings reported at 600 nm. (c) Profilometry for the 20 wt % PMDETA loading at time increments of 10 min, 20 min, 30 min, and 1 h.

polymerization at 10 wt % with respect to monomers. TEA also catalyzes the thiol—thioester exchange; therefore, after the

polymerization, it was subsequently removed to maintain stable microparticles for storage and later use. Microparticles

had an average diameter $(D_{\rm n})$ of 4.0 \pm 0.4 μm with a coefficient of variance (CV) of 10% as determined by ImageJ analysis of optical microscopy (Figure 1b). Particle size distribution is reported in Figure S1. Dynamic scanning calorimetry (DSC) was used to determine the glass transition $(T_{\rm g})$ of the particle network to be -22 °C (Figure S2). Fourier-transform infrared spectroscopy (FTIR) was performed on dry particles to confirm the presence of residual, unreacted thiol and practically complete consumption of the acrylates as seen in Figure S3.

The particle casting and coalescence process is illustrated in Figure 2a, where particles are first cast on a substrate and then compressed with the appropriate stimuli to form a homogeneous cross-linked network. To demonstrate coalescence, dry particles were cast on a glass slide at room temperature. Particles were then swollen with liquid base, N,N,N',N",N"'pentamethyldiethylenetriamine (PMDETA), as the catalyst for the thiol-thioester exchange. PMDETA was selected as the exchange catalyst because it is less volatile than TEA, which was used in the polymerization, and will therefore mitigate evaporation during the coalescence process. In the presence of free thiols, the base deprotonates the free thiol to generate a thiolate anion that is then able to add into the thioester carbonyl (Figure 2b). This reaction then enables bond exchange where the bond to another sulfide is broken, regenerating the thiolate anion, and the reaction persists so long as the base catalyst is present. This behavior results in interparticle bond exchange when two or more particles are in direct contact, inducing coalescence into a homogeneous polymer film. The exchange mechanism is well-understood, and this work builds upon foundational understanding of this reaction from the studies of the thiol-thioester exchange performed by Worrellet al. 24,31 The particles were compressed between two pieces of glass via clamping with binder clips, maintained at ambient conditions, and monitored over time, resulting in free-standing polymer films with a thickness of about 150 μ m after 24 h (Figure 2c).

Optical Characterization. The concentration of PMDE-TA was 5, 10, or 20 wt % relative to the particle weight to control the time scale of bond exchange and coalescence. Optical microscopy was performed to observe the coalescence process over time at the three catalyst loadings seen in Figure 3. Time points include the initial particles just after swelling with base, 1, 6, and 24 h after swelling. Distinct particle boundaries were observed, although there were various indiscernible regions where swollen particles in contact with each other and the glass could not be resolved. Visually, there was a reduction of visible particle boundaries over time with the coalescence of the individual particles. A control was run for 24 h without the addition of a base to confirm a lack of particle coalescence (Figure S4).

In samples containing a base, optical transparency improves over time due to coalescence, which was observed not only in optical microscopy but also quite apparently by eye as well (Figure 4a and Figure S5). This increase in transparency was confirmed by UV—vis (Figure 4b). Transmission was reported at a wavelength of 600 nm. Complete UV—vis spectra are available in Figure S6. Over time, transmission increased until about 3 days. There was very little increase in transmission from three days to seven days, indicating the coalescence process had reached near completion, optically, by the third day. Particle coalescence at the 10 and 20 wt % catalyst loadings showed similar behavior, but the 5 wt % loading was

slower and did not achieve the same final transmission value as the 10 and 20 wt % loadings by the seventh day. UV—vis was run for the control that did not contain a base, with no change to the spectrum from the initial time point to 24 h, confirming a lack of particle coalescence without the presence of the exchange catalyst (Figure S7). These optical characterization techniques measured the behavior through the thickness of the material, with surface measurements presented later. It is important to note that particle deposition was not precisely controlled during casting and swelling. Nonuniform stress fields potentially arose during compression, and some variability was expected in results. The overarching conclusion is that addition of base does induce particle coalescence.

To confirm control of the time scale of bond exchange and coalescence via modulation of the catalyst concentration, stress relaxation experiments were performed on bulk polymer films made from monomers as an analogue to particle bond exchange. Bulk films were polymerized neat utilizing the same monomer stoichiometry used for the particle formulation of 1.4:2 PETMP to TEDA. To mirror the particle polymerization process, the reaction was catalyzed with TEA and allowed to react overnight. TEA was evaporated from the films, and the films were subsequently swollen with indicated amounts of the exchange catalyst, PMDETA. DSC confirmed that the network of the bulk film was representative of the particle network, with the $T_{\rm g}$ of the bulk film measured to be -21 °C, recalling that the $T_{\rm g}$ of the particles was -22 °C (Figure S2). Stress relaxation was performed on rectangular films that were strained to 5% in tension at ambient conditions. The results in Figure S8 conclude that increasing the content of the base increased the rate at which stress relaxation occurred, consistent with previous investigations of thiolthioester exchange studies done by Worrell et al.²⁴ A control was run at ambient conditions after the initial evaporation step that was done to remove the TEA, and no PMDETA was swollen into the film. No stress relaxation was observed as displayed by the flat line in Figure S8. This experiment was performed to confirm that stress relaxation did not occur in this formulation without the presence of a base. This also confirmed the step to evaporate the base from the films was successful, and residual TEA was not responsible for any stress relaxation. Although in optical microscopy and UV-vis, particle coalescence at the 10 and 20 wt % catalyst loadings, as mentioned prior, had comparatively similar behavior, the 20 wt % base concentration was chosen as the representative system to perform further characterization experiments due to the rapid relaxation behavior determined by the bulk film stress relaxation tests. Further investigation into why the 10 and 20 wt % catalyst loadings exhibit similar behavior in the particle configuration as opposed to bulk film stress relaxation would be valuable and could help to determine dependence on swelling behavior at the microscale. While not explored here, another interesting capability that arises is the modulation of particle size, shape, and character, which is readily tailorable due to the body of literature that exists on microparticle polymerization. 32'-34 Investigating the effect CANs particles of various sizes and shapes may have on the coalescence process would be an informative area of study.

Surface Characterization. Profilometry was performed to measure changes in the surface topography of the particle coalescence over time at the glass—particle interface (Figure 4c). Samples were prepared in the same manner as the optical experiments, utilizing 20 wt % PMDETA. To perform surface

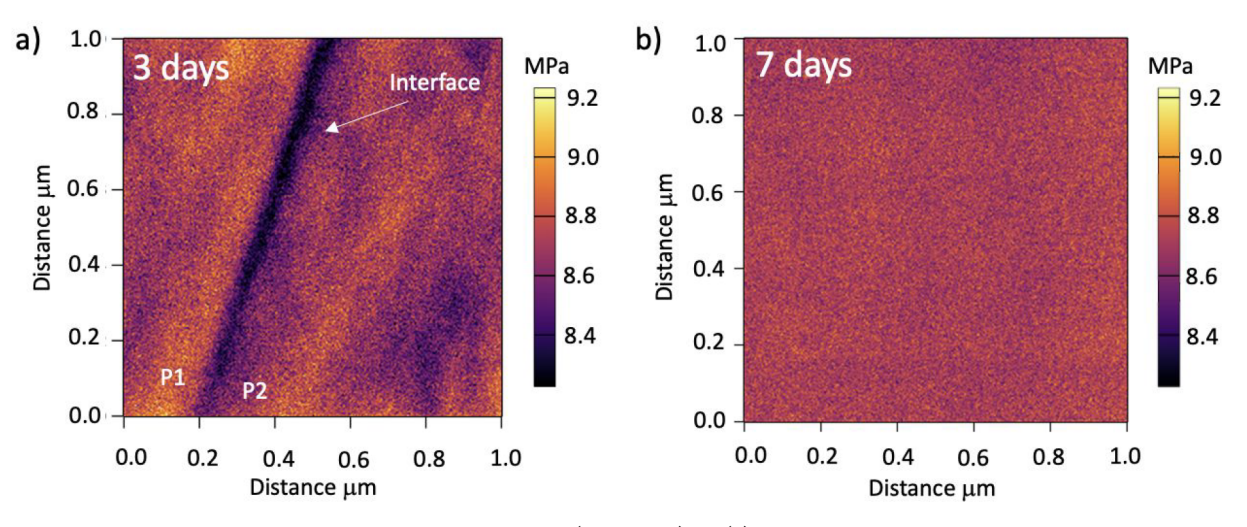


Figure 5. AFM modulus map for an interface between two particles (P1 and P2) at: (a) 3 days, displaying a visible interface between particles and (b) 7 days of compression, displaying homogeneity of the surface modulus.

scans, the clamped sample was opened and the top piece of glass removed. The base was then evaporated at 70 °C for 6 min before scanning, to ensure the liquid base did not confound probe measurements. The surface of the sample was scanned from one edge to the other, PMDETA was readded to the sample, and it was resealed between the glass slides until the next scanning time point. The same sample was tested at 10, 20, and 30 min time points, following the procedure listed above to mitigate the impact of uneven particle deposition between samples on early stages of relaxation. For the 1 h time point, a new sample was used. This was done because opening and closing of the sample has the capacity to decorate the surface of the particles with contaminates and disturb the coalescence behavior, so a pristine sample was used for the longest time point where initial particle deposition will have less impact on results. The 1 h sample was processed and scanned in the same manner as the preceding samples. Profilometry showed the reduction of surface features measured over time on the order of millimeters to microns. At 1 h, films reached a relatively flat surface, although in optical microscopy particle coalescence was occurring up until 24 h, and in the UV-vis, transmission continued to change through the bulk of the material for up to about 3 days (Figure 4c and Figure S6). These results indicate that stresses at the particle and glass interface are potentially higher than through the bulk, resulting in faster relaxation time scales at these interfaces. The effect of strain and stress variation on the exchange rate of dynamic networks has been investigated previously and is an area of interest in the field.³⁵ It is possible that some exchange between particles occurs during the evaporation step while catalyst is still present at elevated temperatures, despite the lack of compressive stresses.²⁴ To determine whether this step was accelerating relaxation behavior substantially, control UVvis experiments were performed on a sample that was clamped between glass and heated to 70 °C for 6 min to replicate the temperature and duration of heating for the profilometry experiments. No substantial change was seen in the spectrum after heating for 30 min (Figure S9a). The same control sample was allowed to coalesce for another 30 min and then heated to 100 °C for 10 min. There was a slight increase of transmission, but it was also observed that the base was being removed from the film (Figure S9b), indicating that processing at too high of temperatures results in the depletion of the base,

which ultimately results in the slowing of bond exchange and particle coalescence once a significant amount of the catalyst is removed. These controls confirm that the heating steps taken to remove base for profilometry measurements are not substantially enhancing stress relaxation or confounding measurements. Overall, profilometry data confirmed that particle surface features reduced to flat surfaces on a shorter time scale than coalescence through the bulk of the material. It also confirms the main phenomenon of this study that particles are coalescing into films.

AFM was performed at the surface of the particle coalescence process at the glass-particle interface to quantify the homogeneity of the network modulus. Optical characterization gave qualitative information about particle coalescence and quantitative light transmission information through the film thickness. Profilometry measured surface topography and was able to scan shorter time points during the coalescence process than AFM, due to the confounding impacts of large topographic features on AFM measurements at early stages of coalescence. AFM fast force mapping was used to measure surface modulus changes over time, which provided insight into changes to the cross-link density between particles. Samples were prepared and measured in the same manner used for profilometry at 20 wt % PMDETA, with detailed explanation on AFM scanning methods reported in the Materials and Methods section. AFM confirmed that surface topography was relatively flat at 1 h, with the height of surface features limited to a length scale of tens of nanometers but continued to evolve over time (Figure S10). Although optical characterization indicated homogeneity at 3 days, the representative modulus map seen in Figure 5a still resulted in a measurable interface between particles at this time point. Interfacial scans taken at five different locations on the film surface all exhibit modulus gradation along the interfaces, but the degree of modulus contrast and geometry exhibited variation (Figure S11), indicating coalescence is nonuniform across the film surface. After 7 days of compression, there were still sub-1 nm topographical features discernible at the particle-particle interfaces (Figure S10), enabling interfaces to be located for modulus mapping. However, the resulting modulus maps were unable to discern any heterogeneity at the interfaces (Figure 5b), so any nonuniformity in modulus is sufficiently small at this point as to be undetectable using force

maps. Different samples were used for the 3 and 7 day time points, as discussed prior so as not to disturb the coalescence process by opening and closing the same sample. The particle coalescence process predicted by Long et al. in a modeling study of vitrimer particle coalescence behavior, reports that interfaces between particles undergo regimes of elevated stress as compared to the bulk particle and eventually result in coalescence.³⁶ Initially, cross-link density may be low between particles, but at sufficient lengths of time, the increase in crosslinking across the interface resulted in modulus values near that of the bulk particle and ultimately resulted in a homogeneous surface. It is also important to recall that coalescence at the glass-particle interface occurred faster than through the bulk, so the modulus through the bulk may not be homogeneous at the same time as the surface.

Interestingly, at 24 h and up to about 7–11 days, the sample had a visibly noticeable heterogeneous appearance through the thickness, having an almost "stained glass" appearance (Figure S12). UV-vis showed relatively unchanging transmission after 3 days although the texture was still visible at 3 days (Figure 4 and Figure S6). It was determined by profilometry and AFM that the surface was relatively flat at this time point, so this phenomenon was likely occurring through the bulk.

Tensile Testing. Uniaxial tensile tests were performed on dog-bone shaped films prepared from particles via the coalescence process. Results were compared with films formed by bulk polymerizations directly from monomer, to discern the integrity of the films generated by the particle coalescence process (Figure 6). First, thioester particles were cast into a

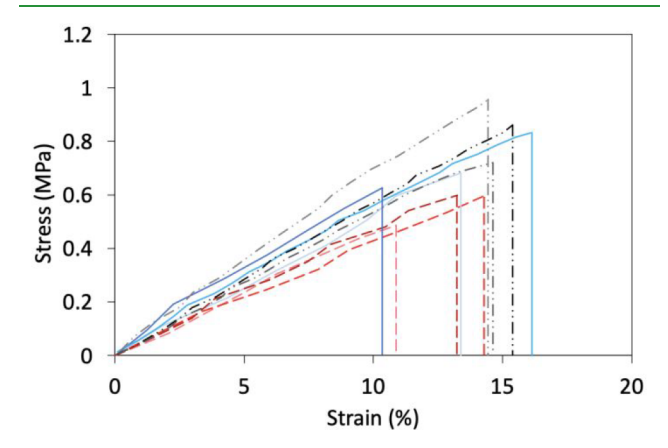


Figure 6. Tensile tests for films prepared from monomer (blue, solid + repeats), particles after 3 days (red, dashed + repeats), and particles after 7 days (black, long dash + repeats).

rectangular shape and 20 wt % PMDETA was added. The sample was then compressed between glass and allowed to coalesce for either 3 or 7 days. At each time point, PMDETA was evaporated from the films via a vacuum oven to halt any dynamic processes thereafter. The results for the 3 and 7 day processed films are depicted in Figure 6 by the red and black curves, respectively, with different shades indicating experimental repeats. Next, bulk films were made directly from monomer, where PETMP and TEDA were mixed with TEA to catalyze the polymerization and immediately cast and compressed between glass. The polymerization proceeded overnight, and the following day, the films were thermally treated in the same manner to remove the TEA. Therefore, all samples subjected to tensile testing no longer contained base. The films

made directly from monomer are represented by the blue curves, with different shades indicating experimental repeats. All resultant films were cut into a dog-bone shape. After processing, the UV-vis spectra for the 3 and 7 days samples were compared to the bulk monomer-films and displayed comparable transmission profiles (Figure S13). It is worth noting that spectra of particle-films before and after thermal processing are relatively unchanged, recalling Figure S6a and compared to Figure S13. As discussed, the optical characterization determined unchanging transmission around 3 days, with thermal treatments thereafter not resulting in any

After 3 days of coalescence time, the modulus and toughness reported in Table 1 are 5 ± 1 MPa and 1.1 ± 0.8 J/m³,

Table 1. Mechanical Properties for Films Made from Monomer and Particles (P) after 3 and 7 Days^a

Film type	M (MPa)	$T (J m^{-3})$	S to B (%)
Monomer	5 ± 1	3 ± 2	13 ± 3
P. 3 days	5 ± 1	1.1 ± 0.8	13 ± 2
P. 7 days	6 ± 1	2 ± 2	14.8 ± 0.5

^aModulus (M) = stress/strain, toughness (T) found by area under the tensile curve, and strain to break (S to B).

respectively, with the modulus being the same as the monomer-film but with a lower toughness. Modulus and toughness for the monomer-film were measured to be 5 ± 1 MPa and $3 \pm 2 \text{ J/m}^3$. After 7 days of coalescence, the particle films appeared to have comparable mechanical properties to that of the films made from monomer with the modulus and toughness of the particle-films being 6 ± 1 MPa and 2 ± 2 J/ m³ respectively. The mechanical properties are comparable and within error, concluding that the films made from particles do not result in compromised integrity after 7 days of coalescence time compared to their counterpart made directly from monomer. From this analysis, it is determined that films made from thioester containing microparticles achieve comparable mechanical properties relative to films directly polymerized from monomer. Particle-films potentially have the advantage of annealing out defects over longer processing times than the bulk monomer-films.

A graphical summary of the results from the particle coalescence study is visualized below in Scheme 1.

Demonstrations. After understanding the coalescence process, a second network was developed without the thioester backbone that yet still contained excess thiol. While this network is not dynamically active on its own, it can participate in surface bond exchange with the particle network through the availability of the excess thiols. The second network was designed with a 1:2 monomer molar ratio of 2,4,6-triallyloxy-1,3,5-triazine (TAT) and hexane dithiol (HDT), achieving a network that contains 33% excess of thiols with a T_g of -55 °C (Figure S14). A thiol-ene polymerization was done to form the network by mixing in photoinitiator Irgacure-819 at 1 wt % to monomers and irradiating the resin with short wavelength visible light. The secondary network and thioester containing microparticles were coupled via interfacial thiol-thioester exchange, seen by the cross-sectional scanning electron microscopy (SEM) images of the joined polymer films (Figure 7). Particles were cast overlapping a rectangular film composed

Scheme 1. Summary of the Particle Coalescence Process and Observations

Time Evolution of Coalescence

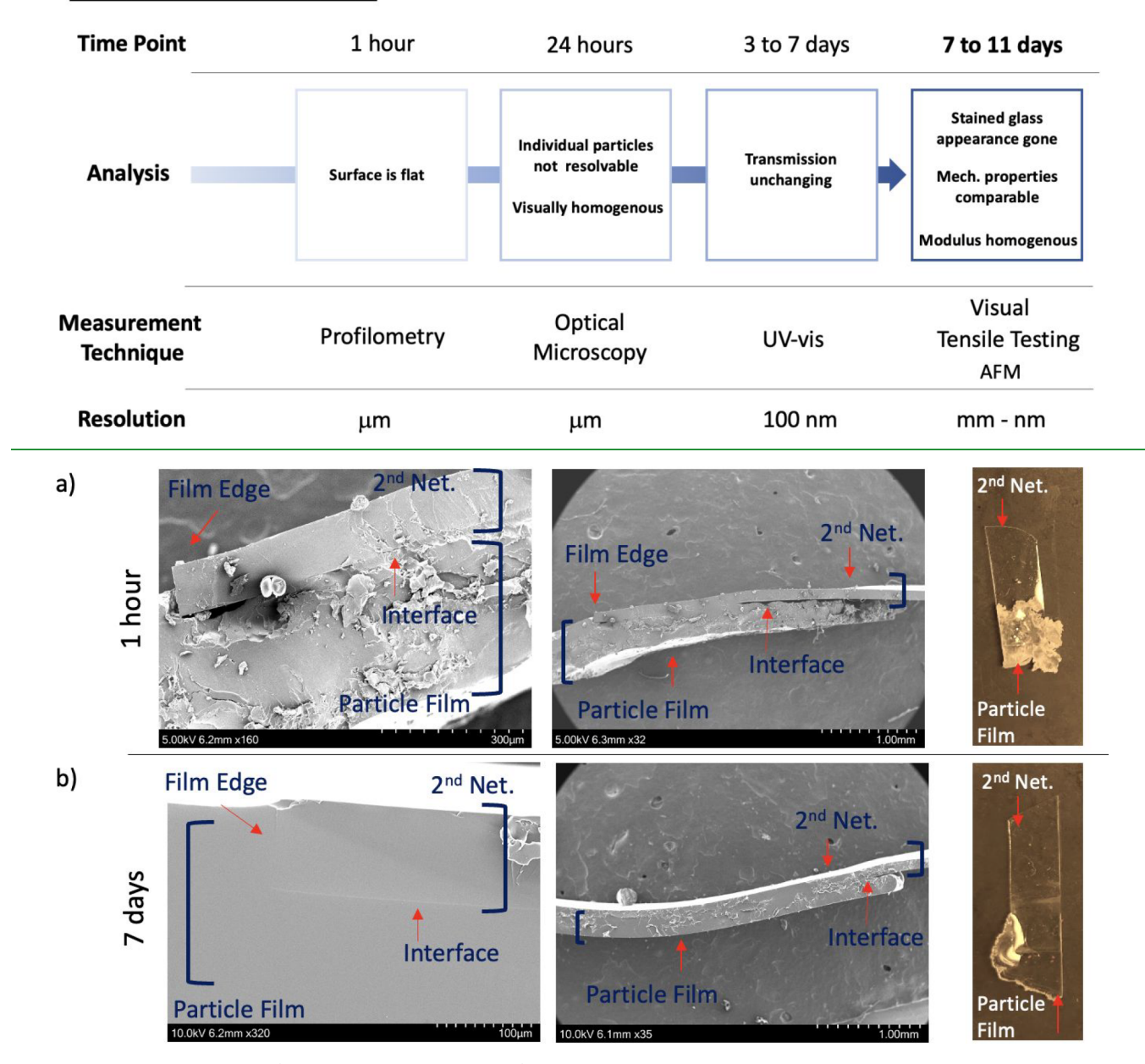


Figure 7. SEM on a cross-section (high mag. left, lower mag. right) of overlapping films from particles welding to the secondary network containing excess thiol (2nd Net. TAT to HDT at a 1:2 ratio) at (a) 1 h, showing a visible interface between the films, and (b) 7 days, with a nearly indiscernible interface between films. The film made from the secondary network is positioned in the top of each photo and the film made from particles is on the bottom. To the right is an image of the joined polymer films at the corresponding weld times with the secondary network toward the top of the image, and the particle film toward the bottom.

of the secondary network (2nd Net.), and PMDETA was added at 20 wt % with respect to particles, to induce bond exchange with the film.

SEM was performed on a cross-section of the overlapping films after 1 h and 7 days of compression to confirm welding between particles and the film. At 1 h, there are noticeable voids between the secondary network and the particle layer (Figure 7a). At 7 days, the two interfaces were almost indiscernible, although at a higher magnification there was still a faintly visible interface (Figure 7b). A control secondary network was designed not containing any excess thiol, with a 1:1.5 monomer molar ratio of TAT to HDT. The particles

were cast on the network followed by the addition of PMDETA, and after 7 days of coalescence, there is still a distinct interface between the two films demonstrating a lack of network integration without the presence of excess thiols (Figure S15). Welding to this secondary network demonstrates the compatibility of these CANs particles with networks of differing chemistries.

Another demonstration was performed to exhibit the spatial control of particle deposition. The thioester particles were selectively deposited along two rectangular strips of the secondary network (Figure 8). PMDETA was added to the

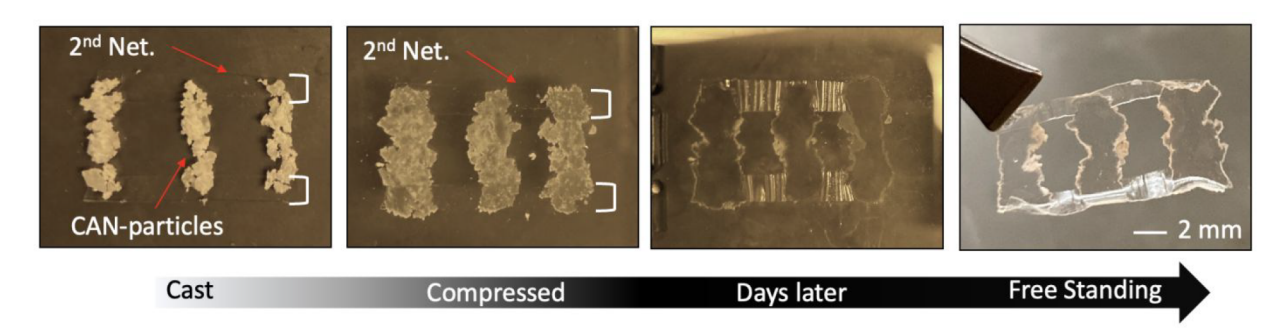


Figure 8. Images of particles being welded to the secondary network in a complex geometry. The particles are initially cast, compressed with base added, and allowed to coalesce and weld over time, resulting in a free-standing polymer film.

particles; the materials were then compressed between glass and allowed to coalesce for 3 days.

After the particles were allowed to coalesce and weld, a freestanding polymer "part" was achieved. There was noticeable deformation to the part due to shrinkage stress, which could be alleviated if the secondary network was also dynamic, enabling stress relaxation through the entirety of both networks and welding sites. Moving forward with this technology, different sets of "writing inks" or microparticles designed with DCCs and varying mechanical properties could be selectively deposited and coalesced together to control resultant mechanical properties in the final material.

CONCLUSION

In conclusion, thioester containing microparticles were synthesized via a thiol-Michael dispersion method. This yielded particles capable of interparticle dynamic covalent bond exchange. The particles designed with an excess of thiol were compressed after the addition of a base catalyst, which resulted in coalescence into homogeneous polymer films. Optical and surface analyses measured and confirmed the particle coalescence into homogeneous polymer films. Uniaxial tensile tests were performed to compare films made from monomer to films made from particles, with the results concluding that there is no compromise to the network integrity after particle coalescence. Mechanical properties of the particle-films are comparable to monomer-films. Furthermore, welding of the particles to a secondary nondynamic network that also contained excess thiols demonstrated the ability for this technology to be utilized for selective particle deposition to result in spatial control of material properties in a resulting polymer film.

MATERIALS AND METHODS

Materials. Pentaerythritol tetrakis (3-mercaptopropionate) (PETMP), triethylamine (TEA), polyvinylpyrrolidone (PVP), 2,4,6triallyloxy-1,3,5-triazine (TAT), hexane dithiol (HDT), and methanol were purchased from Sigma-Aldrich. Irgacure-819 was purchased from iGM resins. Binder clips were purchased from Staples and used brand new.

Thioester Diacrylate (TEDA) Synthesis. Synthesis largely follows that reported and developed by Bowman et al.³⁷

Microparticle Polymerization. Microparticle polymerization was performed as follows with a monomer molar ratio of 1.4:2 PETMP to TEDA to yield a network with excess thiol. PVP (0.09935 g, 50 wt % to monomers) was dissolved in 3.14 mL (2.48 g) of MeOH (8 wt % monomers to solvent). PETMP (0.0913 g, 0.0713 mL) was dissolved. TEDA (0.1074 g, 0.100 mL) was dissolved. The mixture was stirred, and TEA was then added to start the reaction at 0.01987 g (0.0274 mL at 10 wt % to monomers). The reaction ran for 1 h and was then

quenched with 10% excess of acetic acid for 30 min. The mixture was centrifuged at 3000 rpm for 2 min, pouring off the clear supernatant, and subsequently washed and centrifuged 3× with MeOH at 3× the volume and spun at the same conditions. MeOH was largely poured off, and the remaining solvent was allowed to evaporate at ambient conditions for 2 days. The dry particles were then stored in the freezer (−18 °C). The polymerization resulted in a yield of about 90%.

Three hundred particles chosen randomly were analyzed via optical microscope images with ImageJ to determine average diameter (D_n) and coefficient of variance (CV). CV was calculated as CV% = (SD/ $D_{\rm p} \times 100$), where SD = standard deviation. Optical microscopy was done with a Nikon Eclipse Ci.

Bulk Film Polymerization from Particles (Particle Coales**cence).** At ambient conditions, particles were cast on a glass slide. Indicated amounts of PMDETA liquid base were added by wt % with respect to the particles. Ex: 10 mg of particles cast, 5 wt % base -0.5mg of base added, 10 wt % base - 1 mg of base added, 20 wt % base - 2 mg of base added. The particles were then compressed between two pieces of glass using binder clips and 100 μ m spacers. Using 10 mg of particles repeatedly resulted in 150 μ m films despite the spacer thickness used. A package of new binder clips from a single vendor was purchased and utilized solely for this study to mitigate variation in applied pressure.

Bulk Film Polymerization from Monomer. At a 1.4:2 PETMP to TEDA monomer molar ratio, 0.1369 g of PETMP (0.10698 mL) was mixed with 0.1611 g of TEDA (0.150 mL). TEA was added (0.00894 g, 0.0123 mL at 3 wt % to monomers), and the mixture was cast and compressed between glass slides utilizing indicated spacers to control thickness. The films were allowed to react overnight. To remove the TEA, the films were held at 70 °C in a vacuum oven overnight and the following day held at 100 °C for ~2 h while a vacuum was pulled, to remove any remaining TEA, until the mass of the film no longer changed (indicating TEA removal).

Secondary Network for Welding Demonstration. A 1:2 monomer molar ratio of 2,4,6-triallyloxy-1,3,5-triazine (TAT) and hexane dithiol (HDT) was mixed with 1 wt % photoinitiator Irgacure-819 with respect to the monomers. The mixture was cast and compressed between glass using 100 μ m spacers. The resin was irradiated with 400-500 nm light at 70 mW/cm² for 2 min. Twopiece welding demo: A piece of the secondary network was cut. Ten milligrams of particles were cast overlapping and extending beyond the secondary network. Twenty weight percent PMDETA was added to the particles, and the materials were clamped between glass and coalesced for 1 h and a second sample for 7 days. Control - same conditions but monomer molar ratio followed 1:1.5 TAT to HDT. Sample was allowed to weld for 7 days. Complex shape demo: Two strips of the secondary network were laid out. Thirty milligrams of particles were split into three regions, and 20 wt % of PMDETA was added to the particles. The materials were then clamped between glass and allowed to coalesce for 3 days.

SEM. SEM was performed on a Hitachi SU3500. The base was removed from films before imaging.

Ultraviolet-Visible Spectroscopy (UV-vis). UV-vis was run on a Thermo Fisher Scientific Evolution 300. Samples were measured with a xenon lamp in transmittance between 200 and 1000 nm with a scan speed of 240 nm min⁻¹. Data intervals were taken at 1 nm and a bandwidth of 2 nm. A background was run and subtracted from the data.

Profilometry. Samples were prepared as described in (particle coalescence) section using 20 wt % PMDETA. Samples were then opened at each time point (10, 20, and 30 min) and PMDETA was evaporated at 70 °C for 6 min. Samples had a somewhat irregular but relatively circular circumference and were scanned in a single direction from end to end at three separate starting points toward the center to maintain consistency. These three starting points were recorded in an effort to try to rescan the same points on the film. The scanning area was about 4 mm in the scan direction. Samples were reswollen with appropriate amounts of base and clamped again until the next time point was reached, and the same steps were followed to take measurements. For the 1 h sample, this sample was allowed to sit unopened for 1 h, with base removed thereafter and then scanned. The most representative curve was chosen for the series. There was a scan speed 100 s. Scans were run on a Dektak 6m profilometer.

Atomic Force Microscopy (AFM). Atomic force microscopy (AFM) analyses were performed with an Asylum Research Cypher S force microscopy system with an etched silicon tip (Tap300Al-G, 40 N/m spring constant, BudgetSensors, Sofia, Bulgaria). AFM AC air topography mode was used to scan the surface topography and find the interface between particles. The selected AC scan size of 20×20 μm^2 was significantly larger than the particles and allowed for mapping of multiple interfaces. Resonance was driven using a blueDrive laser to mitigate noise in the AC scans, and topographical features associated with interfaces between particles were readily observable even down to the sub-1 nm (z-axis only) magnitudes associated with interface topographies in the 7 day sample (Figure S10). After interface identification, high-resolution fast force mapping (FFM) scans covering a 1 \times 1 μ m² area were performed at 250 Hz with a peak force of 300 nN. Due to the exponential relationship between FFM pixel density and imaging times, the 1 \times 1 μ m² FFM scan size was chosen because it enabled the sub-20 nm spatial resolution, necessary to map interface modulus gradations, to be captured at time scales (approximately 35 min per scan) sufficiently fast to mitigate deleterious impacts of thermomechanical drift in the instrument. FFM force curves were analyzed using a Hertzian contact mechanics model to generate a modulus map at particle interfaces with sub-20 nm spatial resolution. The surface is reported as effectively flat at 3 days, but the measurable surface topography at sub-1 nm served to confirm that measurements were performed at a particle-particle interface with the modulus map reporting homogeneity. Separate samples were prepared for the 3 and 7 day time points. Processing was the same as profilometry experiments.

FTIR. Attenuated total reflectance (ATR)-FTIR was done on dried particles for 32 scans with a resolution of 4. ATR-FTIR was run on a Thermo Fischer Scientific Nicolet iS50 FT-IR.

DSC. The samples (particles or bulk film) were initially heated to 70 °C to erase thermal history and cooled at 5 °C/min to -70 °C, and the test was run from -70 to 70 °C and ramped at 10 °C/min to generate the reported curve. DSC was run on a TA DSC 2500.

DMA. Tests were run on an TA RSA-G2.

Stress Relaxation. Bulk films made from monomers (procedure listed above) were used. Indicated amounts of liquid base PMDETA were swollen into the films postpolymerization. Five weight perscent strain was exacted on the films and run for 2 h at ambient conditions. Control: Bulk films made from monomer with TEA evaporated out as described above were run at the same conditions (100 μ m thick

Stress-Strain. Bulk films made from monomer: Procedure as listed above, utilizing 400 μ m spacers. Bulk films made from particles: Films were prepared as discussed above and allowed to coalesce for 3 and 7 days. To remove PMDETA, the films were held at 70 °C in a vacuum oven overnight and the following day at 100 °C for ~2 h while the vacuum was pulled, to remove any remaining base, until the mass of the film no longer changed (indicating base removal). Dog-bone dimensions for all samples were approximately 12.47 mm \times 2.5 mm \times 0.37 mm (lxwxt). Samples were strained at 0.1 mm/s at ambient conditions and run in triplicate for each polymer film type. Young's modulus was calculated as the slope of the tensile curve (stress/ strain). Toughness was found using the trapezoid rule to find the area under the tensile curve.

ASSOCIATED CONTENT

Supporting Information

The Supporting Information is available free of charge at https://pubs.acs.org/doi/10.1021/acsami.2c05113.

Figures of particle size distribution, DSC traces, FTIR spectra, optical microscopy images, Images of particles coalescing into films for the designated catalyst loadings, UV-vis spectra, stress strain profiles, AFM topography, modulus gradation along various particle interfaces, images of particle coalescence over time and evolution of the "stained glass" appearance, and SEM images (PDF)

AUTHOR INFORMATION

Corresponding Author

Christopher N. Bowman - Department of Materials Science and Engineering and Department of Chemical and Biological Engineering, University of Colorado Boulder, Boulder, Colorado 80309, United States; o orcid.org/0000-0001-8458-7723; Email: Christopher.bowman@colorado.edu

Authors

Alina M. Martinez - Department of Materials Science and Engineering, University of Colorado Boulder, Boulder, Colorado 80309, United States

Lewis M. Cox – Department of Mechanical Engineering, Montana State University, Bozeman, Montana 59717, United States

Amir Darabi - Department of Mechanical Engineering, Montana State University, Bozeman, Montana 59717, United States

Nicholas J. Bongiardina - Department of Materials Science and Engineering, University of Colorado Boulder, Boulder, Colorado 80309, United States

Complete contact information is available at: https://pubs.acs.org/10.1021/acsami.2c05113

The authors declare no competing financial interest.

ACKNOWLEDGMENTS

This work was completed with the financial support of National Science Foundation (NSF) DMR 1809841, NIH grant 1 F31 DE027861-01A1, and NSF funding under grant number CMMI-2038512. The authors would like to thank the CU Boulder COSINC-FAB facility for use of their profilometer. The authors would like to thank CU Boulder COSINC-CHR facility for use of their SEM. The authors would like to thank Professor Tim White's lab, for use of their DSC.

REFERENCES

(1) Ngo, T. D.; Kashani, A.; Imbalzano, G.; Nguyen, K. T. Q.; Hui, D. Additive Manufacturing (3D Printing): A Review of Materials, Methods, Applications and Challenges. Composites Part B: Engineering **2018**, *143*, 172–196.

- (2) Muralidharan, A.; Uzcategui, A. C.; McLeod, R. R.; Bryant, S. J. Stereolithographic 3D Printing for Deterministic Control over Integration in Dual-Material Composites. Adv. Mater. Technol. 2019, 4 (11), 1900592.
- (3) Yu, L.; Lei, Z.; Sun, X.; Ding, P.; Wesche, A.; Jin, Y.; Zhang, W.; Long, R. Rapid Fabrication of Fiber-Reinforced Polyimine Composites with Reprocessability, Repairability, and Recyclability. ACS Appl. Polym. Mater. 2021, 3 (11), 5808-5817.
- (4) Neumann, T. V.; Dickey, M. D. Liquid Metal Direct Write and 3D Printing: A Review. Adv. Mater. Technol. 2020, 5 (9), 2000070.
- (5) Cole, D. P.; Riddick, J. C.; Iftekhar Jaim, H. M.; Strawhecker, K. E.; Zander, N. E. Interfacial Mechanical Behavior of 3D Printed ABS. I. Appl. Polym. Sci. 2016, 133 (30), 43671.
- (6) Collinson, D. W.; Kolluru, P. V.; Von Windheim, N.; Brinson, L. C. Distribution of Rubber Particles in the Weld Zone of Fused Filament Fabricated Acrylonitrile Butadiene Styrene and the Impact on Weld Strength. Additive Manufacturing 2021, 41, 101964.
- (7) Wang, D.; Liang, X.; Russell, T. P.; Nakajima, K. Visualization and Quantification of the Chemical and Physical Properties at a Diffusion-Induced Interface Using AFM Nanomechanical Mapping. Macromolecules 2014, 47 (11), 3761-3765.
- (8) Kline, D. B.; Wool, R. P. Polymer Welding Relations Investigated by a Lap Shear Joint Method. Polym. Eng. Sci. 1988, 28 (1), 52-57.
- (9) Shi, Q.; Yu, K.; Dunn, M. L.; Wang, T.; Qi, H. J. Solvent Assisted Pressure-Free Surface Welding and Reprocessing of Malleable Epoxy Polymers. Macromolecules 2016, 49 (15), 5527-5537.
- (10) Chevalier, Y.; Pichot, C.; Graillat, C.; Joanicot, M.; Wong, K.; Maquet, J.; Lindner, P.; Cabane, B. Film Formation with Latex Particles. Colloid Polym. Sci. 1992, 270 (8), 806-821.
- (11) Keddie, J. L.; Routh, A. F. Fundamentals of Latex Film Formation; Springer, 2010.
- (12) Steward, P. A.; Hearn, J.; Wilkinson, M. C. An Overview of Polymer Latex Film Formation and Properties. Adv. Colloid Interface Sci. 2000, 86 (3), 195-267.
- (13) Mazur, S.; Plazek, D. J. Viscoelastic Effects in the Coalescence of Polymer Particles. Prog. Org. Coat. 1994, 24 (1-4), 225-236.
- (14) Zhan, Y.; Lavorgna, M.; Buonocore, G.; Xia, H. Enhancing Electrical Conductivity of Rubber Composites by Constructing Interconnected Network of Self-Assembled Graphene with Latex Mixing. J. Mater. Chem. 2012, 22 (21), 10464.
- (15) Potts, J. R.; Shankar, O.; Du, L.; Ruoff, R. S. Processing-Morphology-Property Relationships and Composite Theory Analysis of Reduced Graphene Oxide/Natural Rubber Nanocomposites. Macromolecules 2012, 45 (15), 6045-6055.
- (16) Yu, K.; Shi, Q.; Li, H.; Jabour, J.; Yang, H.; Dunn, M. L.; Wang, T.; Qi, H. J. Interfacial Welding of Dynamic Covalent Network Polymers. Journal of the Mechanics and Physics of Solids 2016, 94, 1-17.
- (17) Yang, H.; Yu, K.; Mu, X.; Wei, Y.; Guo, Y.; Qi, H. J. Molecular Dynamics Studying on Welding Behavior in Thermosetting Polymers Due to Bond Exchange Reactions. RSC Adv. 2016, 6 (27), 22476-22487.
- (18) Chen, X.; Dam, M. A.; Ono, K.; Mal, A.; Shen, H.; Nutt, S. R.; Sheran, K.; Wudl, F. A Thermally Re-Mendable Cross-Linked Polymeric Material. Science 2002, 295 (5560), 1698-1702.
- (19) Liu, Y.-L.; Chuo, T.-W. Self-Healing Polymers Based on Thermally Reversible Diels-Alder Chemistry. Polym. Chem. 2013, 4 (7), 2194.
- (20) Cheng, C.; Bai, X.; Zhang, X.; Li, H.; Huang, Q.; Tu, Y. Self-Healing Polymers Based on a Photo-Active Reversible Addition-Fragmentation Chain Transfer (RAFT) Agent. J. Polym. Res. 2015, 22 (4), 46.
- (21) Yao, L.; Rong, M. Z.; Zhang, M. Q.; Yuan, Y. C. Self-Healing of Thermoplastics via Reversible Addition-Fragmentation Chain Transfer Polymerization. J. Mater. Chem. 2011, 21 (25), 9060.
- (22) Robinson, L. L.; Self, J. L.; Fusi, A. D.; Bates, M. W.; Read de Alaniz, J.; Hawker, C. J.; Bates, C. M.; Sample, C. S. Chemical and Mechanical Tunability of 3D-Printed Dynamic Covalent Networks Based on Boronate Esters. ACS Macro Lett. 2021, 10 (7), 857–863.

- (23) Fu, F.; Huang, M.; Zhang, W.; Zhao, Y.; Liu, X. Thermally Assisted Self-Healing Behavior of Anhydride Modified Polybenzoxazines Based on Transesterification. Sci. Rep 2018, 8 (1), 10325.
- (24) Worrell, B. T.; McBride, M. K.; Lyon, G. B.; Cox, L. M.; Wang, C.; Mavila, S.; Lim, C.-H.; Coley, H. M.; Musgrave, C. B.; Ding, Y.; Bowman, C. N. Bistable and Photoswitchable States of Matter. Nat. Commun. 2018, 9 (1), 2804.
- (25) Zheng, M.; Guo, Q.; Yin, X.; Getangama, N. N.; de Bruyn, J. R.; Xiao, J.; Bai, Y.; Liu, M.; Yang, J. Direct Ink Writing of Recyclable and in Situ Repairable Photothermal Polyurethane for Sustainable 3D Printing Development. J. Mater. Chem. A 2021, 9 (11), 6981-6992.
- (26) Shi, Q.; Yu, K.; Kuang, X.; Mu, X.; Dunn, C. K.; Dunn, M. L.; Wang, T.; Jerry Qi, H. Recyclable 3D Printing of Vitrimer Epoxy. Mater. Horiz. 2017, 4 (4), 598-607.
- (27) Brown, T. E.; Carberry, B. J.; Worrell, B. T.; Dudaryeva, O. Y.; McBride, M. K.; Bowman, C. N.; Anseth, K. S. Photopolymerized Dynamic Hydrogels with Tunable Viscoelastic Properties through Thioester Exchange. Biomaterials 2018, 178, 496-503.
- (28) Sowan, N.; Cox, L. M.; Shah, P. K.; Song, H. B.; Stansbury, J. W.; Bowman, C. N. Dynamic Covalent Chemistry at Interfaces: Development of Tougher, Healable Composites through Stress Relaxation at the Resin-Silica Nanoparticles Interface. Adv. Mater. Interfaces 2018, 5 (18), 1800511.
- (29) Huang, Q.; Tang, Z.; Wang, D.; Wu, S.; Guo, B. Engineering Segregated Structures in a Cross-Linked Elastomeric Network Enabled by Dynamic Cross-Link Reshuffling. ACS Macro Lett. 2021, 10 (2), 231-236.
- (30) Lu, L.; Pan, J.; Li, G. Recyclable High-Performance Epoxy Based on Transesterification Reaction. J. Mater. Chem. A 2017, 5 (40), 21505-21513.
- (31) Worrell, B. T.; Mavila, S.; Wang, C.; Kontour, T. M.; Lim, C.-H.; McBride, M. K.; Musgrave, C. B.; Shoemaker, R.; Bowman, C. N. A User's Guide to the thiol-thioester Exchange in Organic Media: Scope, Limitations, and Applications in Material Science. Polym. Chem. 2018, 9 (36), 4523-4534.
- (32) Wang, C.; Podgórski, M.; Bowman, C. N. Monodisperse Functional Microspheres from Step-Growth "Click" Polymerizations: Preparation, Functionalization and Implementation. Mater. Horiz. **2014**, 1 (5), 535–539.
- (33) Wang, C.; Zhang, X.; Podgórski, M.; Xi, W.; Shah, P.; Stansbury, J.; Bowman, C. N. Monodispersity/Narrow Polydispersity Cross-Linked Microparticles Prepared by Step-Growth Thiol-Michael Addition Dispersion Polymerizations. Macromolecules 2015, *48* (23), 8461–8470.
- (34) Huang, Y.; Yuan, J.; Tang, J.; Yang, J.; Zeng, Z. One Step Synthesis of Monodisperse Thiol-Ene Clickable Polymer Microspheres and Application on Biological Functionalization. Eur. Polym. J. 2019, 110, 22-30.
- (35) De Alwis Watuthanthrige, N.; Ahammed, B.; Dolan, M. T.; Fang, Q.; Wu, J.; Sparks, J. L.; Zanjani, M. B.; Konkolewicz, D.; Ye, Z. Accelerating Dynamic Exchange and Self-Healing Using Mechanical Forces in Crosslinked Polymers. Mater. Horiz. 2020, 7 (6), 1581-1587.
- (36) Yu, L.; Sun, X.; Jin, Y.; Zhang, W.; Long, R. Mechanics of Vitrimer Particle Compression and Fusion under Heat Press. International Journal of Mechanical Sciences 2021, 201, 106466.
- (37) Podgórski, M.; Huang, S.; Bowman, C. N. Additive Manufacture of Dynamic Thiol-Ene Networks Incorporating Anhydride-Derived Reversible Thioester Links. ACS Appl. Mater. Interfaces 2021, 13 (11), 12789-12796.